

## MIT Open Access Articles

*Real-time, sensitive electrical detection of Cryptosporidium parvum oocysts based on chemical vapor deposition-grown graphene*

The MIT Faculty has made this article openly available. **Please share** how this access benefits you. Your story matters.

**Citation:** It Wong, Jen, Lu Wang, Yumeng Shi, Tomás Palacios, Jing Kong, Xiaochen Dong, and Hui Ying Yang. "Real-Time, Sensitive Electrical Detection of Cryptosporidium Parvum Oocysts Based on Chemical Vapor Deposition-Grown Graphene." Appl. Phys. Lett. 104, no. 6 (February 10, 2014): 063705. © 2014 AIP Publishing.

**As Published:** <http://dx.doi.org/10.1063/1.4864154>

**Publisher:** American Institute of Physics

**Persistent URL:** <http://hdl.handle.net/1721.1/87553>

**Version:** Final published version: final published article, as it appeared in a journal, conference proceedings, or other formally published context

**Terms of Use:** Article is made available in accordance with the publisher's policy and may be subject to US copyright law. Please refer to the publisher's site for terms of use.



## Real-time, sensitive electrical detection of *Cryptosporidium parvum* oocysts based on chemical vapor deposition-grown graphene

Jen It Wong, Lu Wang, Yumeng Shi, Tomás Palacios, Jing Kong, Xiaochen Dong, and Hui Ying Yang

Citation: [Applied Physics Letters](#) **104**, 063705 (2014); doi: 10.1063/1.4864154

View online: <http://dx.doi.org/10.1063/1.4864154>

View Table of Contents: <http://scitation.aip.org/content/aip/journal/apl/104/6?ver=pdfcov>

Published by the [AIP Publishing](#)

---

### Articles you may be interested in

[Taylor series expansion based multidimensional image reconstruction for confocal and 4 p i microscopy](#)  
*Appl. Phys. Lett.* **103**, 073702 (2013); 10.1063/1.4817928

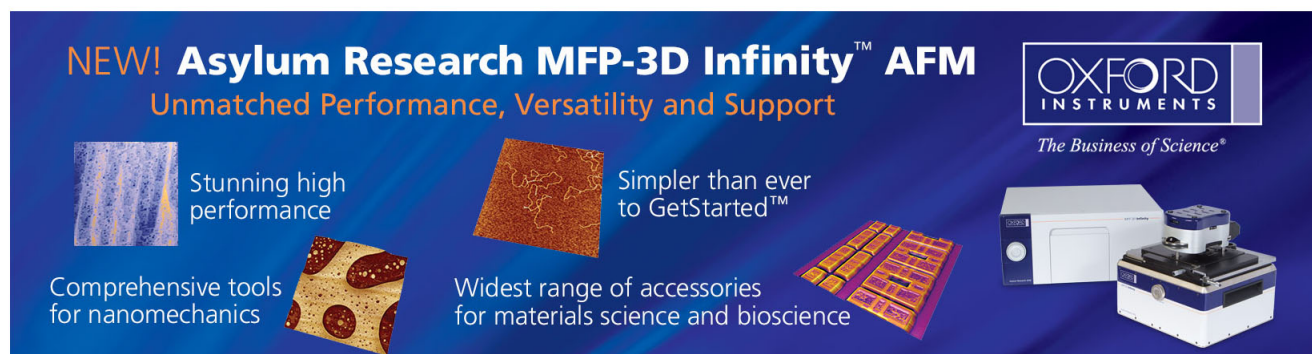
[A microfluidic platform for real-time and in situ monitoring of virus infection process](#)  
*Biomechanics* **6**, 034122 (2012); 10.1063/1.4756793

[Plasmon-polaritons on graphene-metal surface and their use in biosensors](#)  
*Appl. Phys. Lett.* **100**, 213110 (2012); 10.1063/1.4721453

[Electrical detection of the biological interaction of a charged peptide via gallium arsenide junction-field-effect transistors](#)  
*J. Appl. Phys.* **103**, 114510 (2008); 10.1063/1.2936853

[Detection of bacterial cells and antibodies using surface micromachined thin silicon cantilever resonators](#)  
*J. Vac. Sci. Technol. B* **22**, 2785 (2004); 10.1116/1.1824047

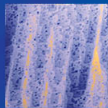
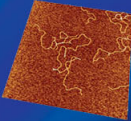
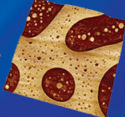


---



**NEW! Asylum Research MFP-3D Infinity™ AFM**  
Unmatched Performance, Versatility and Support

**OXFORD INSTRUMENTS**  
*The Business of Science®*

Stunning high performance  
Simpler than ever to GetStarted™  
Comprehensive tools for nanomechanics  
Widest range of accessories for materials science and bioscience

## Real-time, sensitive electrical detection of *Cryptosporidium parvum* oocysts based on chemical vapor deposition-grown graphene

Jen It Wong,<sup>1,2</sup> Lu Wang,<sup>3</sup> Yumeng Shi,<sup>2</sup> Tomás Palacios,<sup>4</sup> Jing Kong,<sup>4</sup> Xiaochen Dong,<sup>1,a)</sup> and Hui Ying Yang<sup>2,b)</sup>

<sup>1</sup>Jiangsu-Singapore Joint Research Center for Organic/Bio-Electronics & Information, Displays and Institute of Advanced Materials (IAM), Nanjing Tech University, 30 South Puzhu Road, Nanjing 211816, China

<sup>2</sup>Pillar of Engineering Product Development, Singapore University of Technology and Design, Singapore 138682

<sup>3</sup>Department of Chemistry and Chemical Biology, Harvard University, Cambridge, Massachusetts 02138, USA

<sup>4</sup>Department of Electrical Engineering and Computer Science, Massachusetts Institute of Technology, 77 Massachusetts Avenue, Cambridge, Massachusetts 02139, USA

(Received 13 December 2013; accepted 5 January 2014; published online 12 February 2014)

*Cryptosporidium parvum* is a common intestinal parasitic protozoan that causes gastroenteritis in man and animals. It poses high risks to drinking water supply because of its ubiquitous distribution in water and their oocysts are resistant to harsh environment conditions. In this work, we demonstrated the use of large-size chemical vapor deposition (CVD) grown graphene films configured as field-effect device for rapid electrical detection of *Cryptosporidium parvum* oocysts (Cp. oocysts). The presence of Cp. oocysts causes the change in the transport characteristics of the antibody-functionalized graphene device, which can be measured in terms of the dependence of the drain current on the sweep of the gate voltage or the real-time drain current data under a constant gate voltage. The high sensor sensitivity of 25 oocysts per milliliter solution and good specificity were evaluated, indicating it a promising candidate for detecting waterborne pathogens in water quality control. © 2014 AIP Publishing LLC. [<http://dx.doi.org/10.1063/1.4864154>]

The recent interests in graphene-based sensors can be attributed to their higher sensitivity,<sup>1</sup> higher conductivity,<sup>2</sup> and larger detection area<sup>3</sup> compared to carbon nanotube-based devices. Redox enzyme-modified chemical vapor deposition (CVD) grown graphene for glucose and glutamate detection<sup>4</sup> and DNA hybridization detection<sup>5</sup> are some examples of graphene-based biosensors. In view of recent progress in graphene-based biosensors,<sup>6–8</sup> we use functionalized graphene as the active sensing material to detect the *Cryptosporidium parvum* (Cp.) at its oocyst stage of proliferation.

*Cryptosporidium parvum*<sup>9</sup> is an ubiquitous intestinal parasitic protozoan that causes gastroenteritis in man and lower animals. It presents a serious threat to human health because of its ubiquitous distribution in water where it can remain viable for infection even after 6–8 months and their oocysts are resistant to harsh environment conditions. Standard procedures<sup>10</sup> such as EPA method 1622 and 1623 are typically used to process the contaminated water. Conventionally, *Cryptosporidium* oocysts can be detected by acid-fast staining,<sup>11</sup> immunofluorescent (IF) antibody staining,<sup>12</sup> flow cytometry,<sup>13</sup> and polymerase chain reaction (PCR).<sup>14,15</sup> Each of the detection techniques<sup>16</sup> has different features and the most frequently used detection method is acid-fast staining. Different acid-fast staining methods have various degrees of sensitivity and specificity and it requires a specialized microscopist to perform the analysis. In addition, immunofluorescent (IF) antibody staining is also frequently used to detect Cp. oocyst, but the non-specificity of the antibody due to the cross reaction with other species might be a problem and this

method requires a large number of oocysts ranging from 50 000–500 000 oocysts/g in order to give a positive detection feedback. Flow cytometry features higher sensitivity than acid-fast staining and IF but it requires an expensive flow cytometry equipment in order to carry out such analysis.<sup>17</sup> As for the case of polymerase chain reaction (PCR), it also features a highly sensitive detection feedback, which is able to detect oocysts number ranging from 100–1000 oocysts/g. However, this process is time consuming and the chemical needed is relatively expensive compared to other methods.

In this work, we demonstrated the use of large-size CVD grown graphene film configured as field-effect device<sup>18</sup> for detecting *Cryptosporidium parvum* oocysts (Cp. oocysts) by monitoring the drain current of the device. The change in the graphene device drain current was caused by the specific binding of Cp. oocysts to the antibodies that were immobilized onto the graphene film surface. From our experimental results, our detection method features high sensitivity and almost instant detection feedback for Cp. oocysts. As few as 100 Cp. oocysts suspended in 4 ml PBS solution can be detected. This study indicated that biofunctionalized graphene field-effect biosensor is a promising candidate for the detection of the Cp. oocysts.

Functionalization of graphene surface via various covalent and noncovalent interactions with graphene has been an area of extensive research.<sup>19</sup> Most recently, techniques such as plasma treatments<sup>20</sup> are also used to enhance the wettability of graphene<sup>21</sup> and to create active sites for the immobilization of biomolecules.<sup>22</sup> In our experiment, we chose the noncovalent bio-functionalization scheme via  $\pi$ -interactions,<sup>23,24</sup> as it is a common and effective method to attach functional groups to graphene surface without disturbing the

<sup>a)</sup>E-mail: iamxcdong@njut.edu.cn

<sup>b)</sup>E-mail: yanghuiying@sutd.edu.sg

electronic properties. First, the device was incubated in a 5 mM linker molecule (1-pyrenebutanoic acid succinimidyl ester, i-DNA Biotechnology) solution in dimethylformamide (DMF) for 2 h at room temperature, and washed with pure DMF and DI water. Second, the linker-modified graphene was then incubated with an as-purchased antibody reagent (A400FLR-1X, Waterborne Inc.) overnight at 4 °C. This antibody reagent consists of a fluorescein-labeled (bright apple green when viewed under a fluorescence microscope) mouse monoclonal antibody made to oocyst outer wall antigenic sites (epitopes) of *Cryptosporidium parvum* (Cp.). After the incubation, the device was rinsed three times in DI water to wash away excess reagent.

The transport properties of the graphene field-effect device after biofunctionalization were measured by sweeping the liquid gate voltage  $V_g$  from 1.0 V to  $-1.0$  V (Figure S1).<sup>18</sup> The liquid gate voltage was applied through a Ag/AgCl wire that was in contact with the buffer solution covering the device. In order to confirm the stability of the graphene field-effect biosensor, three additional sweeps were carried out after the first transport measurement. The transfer curves overlaid on each other and there was no obvious shape change for various  $V_g$  sweeps, which confirmed the good stability of the device. Moreover, only devices that could reproduce stable and repeatable  $I_d$ - $V_g$  curves were chosen for sensing experiments.

The CVD-grown graphene sheet used for device fabrication was characterized with Raman spectroscopy and atomic force microscopy (AFM), and the results are shown in Figures 1(a) and 1(b), respectively. The mono-layered and few-layered graphene domains were verified by the characteristic G/2D Raman peaks.<sup>25</sup> The inset of Figure 1(a) shows the photo of the fabricated field-effect device with the graphene sheet in contact with two separate electrodes.

To convert the graphene device to a biosensor, the non-covalent bio-functionalization of the graphene surface was

carried out, with the steps illustrated in Figure 1(c). In order to verify the immobilization of the antibodies onto the graphene surface, a fluorescence image was taken after the functionalization and Figure 1(d) shows the super-imposed fluorescence microscopy image on top of an optical microscopy image of the same device area. The image showed that only the area with the graphene sheet was immobilized with the fluorescein-labeled antibody reagents which appeared bright apple green, and that the quartz substrate was not modified with the antibodies.

The schematic of the graphene-based field-effect biosensor configuration is illustrated in Figure 2, with the photo of an actual device in the left inset. The homebuilt PDMS (Polydimethylsiloxane) flow cell provided a controlled liquid environment for the Cp. oocyst containing solution to interact with the active sensing area of the device. The PDMS flow cell was built before any bio-modification to the device. The right inset of Figure 2 shows SEM image and fluorescence microscopy image of a single Cp. oocyst (scale bar = 2  $\mu$ m).

For Cp. oocysts sensing tests, various concentrations of Cp. oocysts were delivered into the PDMS flow cell in buffer solutions consisting of PBS with antibiotics (penicillin, streptomycin, and gentamicin), Amphotericin B, and 0.01% Tween 20, and the electrical measurement for the presence of Cp. oocysts was carried out. The solutions were delivered with a flow rate of 0.30 ml/h through the PDMS channel. The antibody is genus-specific and binds only to the oocysts if they are present.

Two sensing methods were used to characterize the change in the graphene field-effect device drain current in response to the presence of Cp. oocysts. In the first method, two minutes after each solution of the Cp. oocysts was delivered into the flow cell, the transfer curve was measured by sweeping the liquid gate voltage ( $V_g$ ) from 1.0 V to  $-1.0$  V with a Ag/AgCl wire in contact with the solution, and monitoring the drain current ( $I_d$ ) while the source-drain voltage

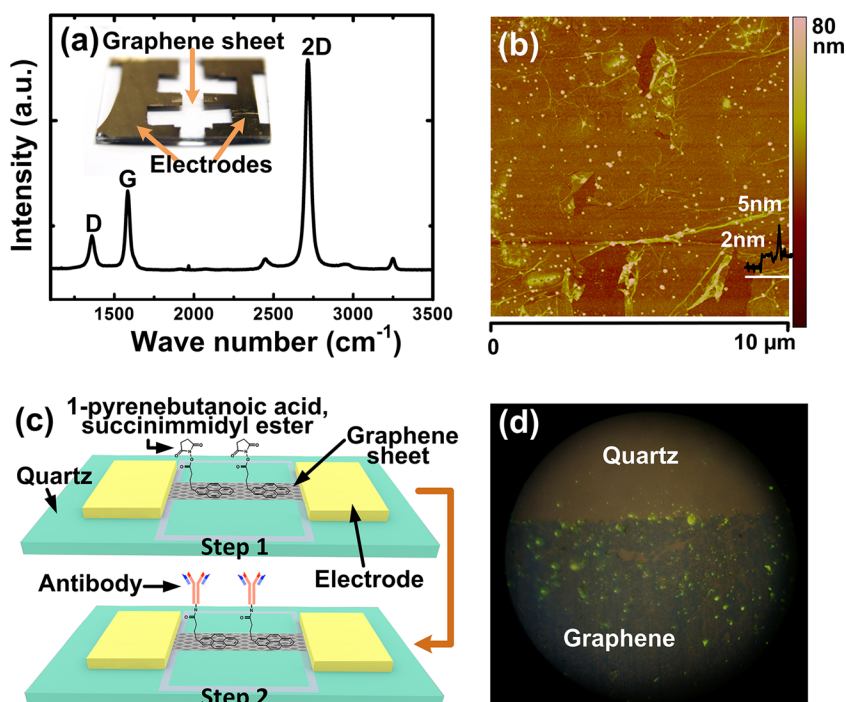


FIG. 1. Graphene sheet characterization and surface bio-functionalization with antibodies. (a) Raman spectrum showing mono-layered and few-layered graphene domains of the graphene sheet. Inset shows the photo of the fabricated field-effect device with the graphene sheet in contact with two separate electrodes. (b) AFM topography of the graphene sheet. (c) Schematic of the non-covalent immobilization of antibodies on graphene surface. (d) Fluorescence microscopy image and optical microscopy image of the same device area super-imposed on each other, taken after biofunctionalization, confirms that only the area with the graphene sheet was immobilized with the fluorescein-labeled antibody reagents which appeared bright apple green, and that the quartz substrate was not modified with the antibodies.

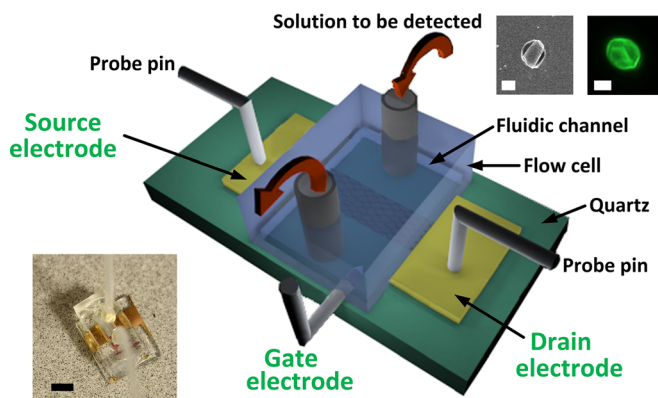


FIG. 2. Schematic of the sensor configuration with the PDMS flow cell and the probe pins for connecting the sensor device to the electrical measurement system. Left inset shows the photo of the actual home-built sensor without the probe pins and Ag/AgCl gate electrode, scale bar = 6 mm. Right inset shows the SEM image and fluorescence microscopy image of a single Cp. oocyst, scale bar = 2  $\mu\text{m}$ .

( $V_{sd}$ ) was kept constant at 0.5 V. The transfer curves were then compared with each other to show the trend of drain current change. In the second method, real-time monitoring of the drain current  $I_d$  under constant  $V_{sd}$  and  $V_g$  was carried out as solutions of different concentrations of Cp. oocyst were delivered into the flow cell consecutively.

In the sensing experiment using the first method, the transfer curves of the functionalized graphene device in solutions containing various concentrations of Cp. oocyst were measured, and the data are plotted in Figure 3. The drain current of our graphene device exhibited ambipolar behavior as a function of the liquid gate voltage ( $V_g$ ) applied to the solution. The initial ambipolar transfer curve measured in buffer solution without Cp. oocyst is shown in black in the figure; and as we delivered into the flow cell a series of increasing concentrations of Cp. oocyst from  $10^3$ ,  $10^4$ ,  $10^5$  to  $10^6$  (oocysts per 4 ml), we observed that the slope of both branches of the ambipolar transfer curve increased. This increasing slope also means that, at a fixed  $V_g$ , the  $I_d$  increases as the Cp. oocyst

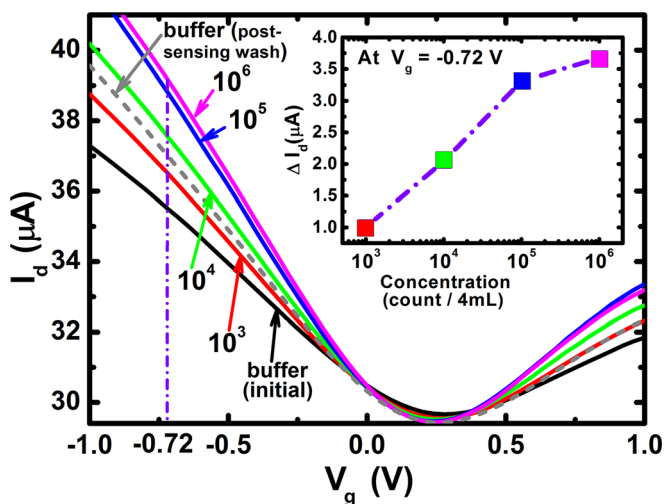


FIG. 3. Electrical detection of Cp. oocysts by monitoring the transfer curves of the functionalized graphene field-effect biosensor in response to various concentrations of Cp. oocyst (count/4ml). Inset: the binding curve showing the concentration dependence of the change in drain current ( $\Delta I_d$ ) at  $V_g = -0.72$  V.

concentration increases, and this concentration dependence of the change in drain current ( $\Delta I_d$ ) at a fixed  $V_g$  (for example, when the liquid gate voltage  $V_g$  was swept to the voltage of  $-0.72$  V) is summarized in the binding curve shown in Figure 3 inset. We can see from the binding curve that the dynamic range of Cp. oocyst sensing was  $10^3$ – $10^6$  (oocysts per 4 ml), as the binding curve saturated at higher concentration range (around  $10^5$ – $10^6$ ). However, looking at the trend of the transfer curves in Figure 3, we believe a sensitivity of  $10^2$  (oocysts per 4 ml) could be achieved. In addition, we also observed the unbinding signal of Cp. oocysts upon buffer washing after the sensing of Cp. Oocyst, shown as dotted grey line in Figure 3. The transfer curve after washing lied somewhere between those for Cp. oocyst with concentrations of  $10^3$  and  $10^4$ , indicating there were some Cp. oocysts that irreversibly adsorbed onto the graphene sheet.

In terms of the sensing mechanism of our graphene device, since both graphene and single-walled carbon nanotubes (SWNTs) are formed by  $sp^2$ -bonded carbons, it is highly possible that the sensing mechanisms for the carbon-based materials are similar. Previously suggested mechanisms in SWNT sensors are electrostatic gating, changes in gate coupling, carrier mobility, and Schottky barrier effect.<sup>26</sup> First, we examine the electrostatic gating sensing mechanism by comparing the transfer curve change pattern of the non-functionalized versus the functionalized graphene field-effect devices in response to the Cp. oocysts in buffer solutions. Figures S2(a) and S2(b)<sup>18</sup> show the response of the pristine graphene device to the Cp. oocysts in buffer solutions. All the transfer curves left-shifted, suggesting the Cp. oocysts adsorbed onto the graphene surface acted as a positive gate through the electrostatic gating mechanism. We also examined the shifts of transfer curves of the functionalized device, and the zoom-in of Figure 3 (Figure S2(c))<sup>18</sup> is for this purpose. Comparing the transfer curve behaviors of the functionalized and the non-functionalized graphene devices (Table I),<sup>18</sup> the left-shift of the minimum conductance point for the functionalized device is far less significant than that of the non-functionalized device: for example, in response to the  $10^4$  (count/4 ml) Cp. oocysts in buffer solution, the minimum conductance point left-shifted by 0.17 V for the non-functionalized device, in contrast to only 0.031 V for the functionalized device. The reduced electrostatic gating effect in the case of the functionalized device compared to bare graphene may be due to the presence of the antibody modification layer between the graphene surface and Cp. oocysts in the case of functionalized device. Second, upon the analysis of the slopes of both the n- and p-branches of the ambipolar transfer curve, we think the dominating sensing mechanism of the functionalized device is the change in the gate couple efficiency.<sup>26,27</sup> In the functionalized device (Table S1),<sup>18</sup> the slope of both n- and p-branches increased significant as the concentration of Cp. oocysts increased, for example, an average of 73% increase in  $10^5$  (counts/4 ml) Cp. Oocyst solution, compared to an average of 25% increase in the non-functionalized device for the same Cp. oocyst concentration. Further work is necessary to elucidate the details on how the binding of Cp. oocysts to the antibody modification layer on the graphene surface changed the electrochemical double-layer capacitance of the graphene-liquid interface. Third, considering the fact that, for

our graphene devices, the electrodes/graphene contact junctions have all been passivated with PDMS from any exposure to solutions, the Schottky barrier mechanism is ruled out in our case. Finally, the change in carrier mobility is unlikely to explain the sensing mechanism because the conductance in both the p- and n-branches was observed to increase whereas the mobility mechanism predicts a conductance decrease as the adding of Cp. oocysts is expected to introduce more carrier scattering centers and hence reduce carrier mobility. In summary, we conclude the underlying sensing mechanism of our graphene biosensor is not simply the effect of electrostatic gating but is mainly due to the interfacial capacitance change.

Besides the detection of Cp. oocyst with the first method of comparing transfer curves (sweeping liquid gate  $V_g$  while keeping  $V_{sd}$  constant) under different target concentrations, we also tested the second method—monitoring in real time the steplike response of the device current (with constant  $V_{sd}$  and  $V_g$ ) to different target concentrations. It is worth pointing out that the experimental results in Figure 3 demonstrated the importance of choosing the liquid gate potential  $V_g$  in the second method: depending on the value of  $V_g$  that was applied during a real-time sensing experiment of Cp. oocyst, the magnitude and even sign of the  $I_d$  change can vary.<sup>28</sup> We chose  $V_g = -0.6$  V to carry out the real-time sensing experiment using another functionalized graphene device with similar transport performance, and the results were shown in Figure 4(a). The  $I_d$  recorded in the first 366 s was the baseline value when the graphene device was in contact with buffer solution. All the buffer solutions used in this real-time sensing experiment were ten times diluted from the one that we used for the transfer curve measurements. The Debye length is longer in diluted buffer, so the sensitivity of the graphene field-effect device could be pushed further by decreasing the screening effect of ions. The first arrow in Figure 4(a) marked the time when the rear end of the tubing leading to the PDMS channel was switched from connecting with pure buffer to the solutions of  $10^2$  Cp. oocyst per 4 ml buffer. The conductance after the switching point fluctuated for  $\sim 1000$  s and then showed a more significant increase and reached a steady plateau. The measurement of the  $I_d$  was interrupted for a while due to the limitation of our data recording system. Nevertheless, it was clearly shown that the presence of Cp. oocyst in the solution caused an increase in the drain current, and this was consistent with what we observed in the first sensing method with the transfer curve measurement. The second and third arrows in Figure 4(a) marked the time that the tubing was switched to the solutions of  $10^3$  and then  $10^4$  Cp. oocyst per 4 ml buffer. As the concentration of the Cp. oocyst increased, the conductance showed a sharper increase in a shorter time compared to its response to  $10^2$  Cp. oocyst per 4 mL buffer. Figure 4(a) inset summarized the concentration dependence of the change in drain current ( $\Delta I_d$ ) when the liquid gate voltage  $V_g$  was at  $-0.6$  V. This sensing experiment showed the feasibility of rapid detection of Cp. oocyst in a liquid sample within 15  $\sim$  30 min, and the consumption of sample volume was only sub-milliliter. The device demonstrated very high sensitivity by showing clear signals to Cp. oocyst solution with concentration down to  $10^2$  per 4 ml solution (which is about

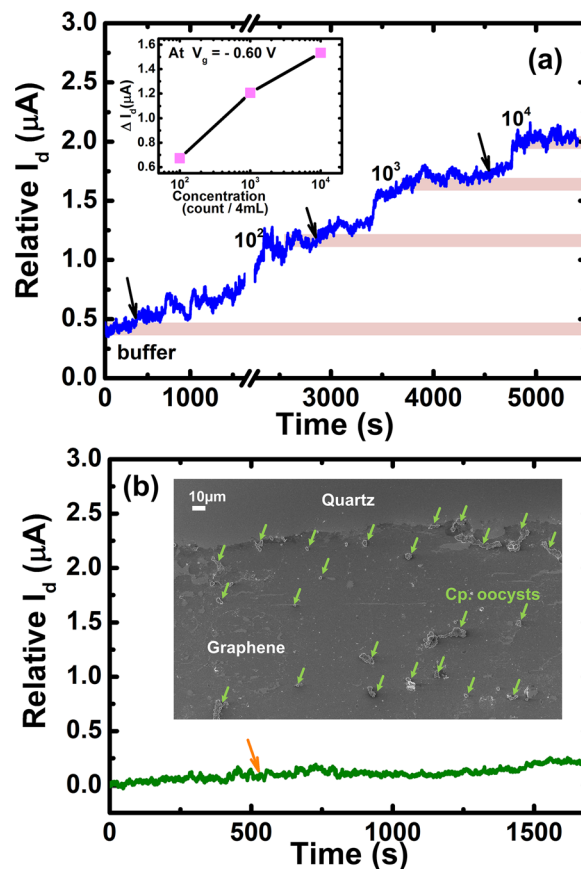


FIG. 4. Real-time Cp. oocyst sensing with high sensitivity and specificity. (a)  $I_d$  vs. time during real-time sensing: solutions delivered into the PDMS channel are firstly buffer, then  $10^2$ ,  $10^3$  and  $10^4$  Cp. oocyst per 4 ml solutions (the starting time of delivering the latter three solutions were marked by arrows). The measurement of the  $I_d$  was interrupted for a while around 1650 s–2250 s due to the limitation of our data recording system. (b) Control sensing experiment against *Giardia lamblia* cysts: the orange arrow marked the time when the solution was switched from buffer to  $10^5$  *Giardia lamblia* cysts per 4 ml solution, and no significant conductance change was observed. Inset: the SEM image confirming the presence of Cp. oocysts on the graphene after the electrical measurement.

25 counts/gram) as well as high selectivity by showing no response to  $10^5$  *Giardia lamblia* cysts per 4 ml solution, another pathogenic protozoa commonly present in water (shown in Figure 4(b)). In addition, scanning electron microscopy (SEM) images were taken in order to verify the presence of Cp. oocysts after the electrical signal was measured. The inset from Figure 4(b) showed that Cp. oocysts were observed on the graphene sheet. All SEM images were taken after the electrical measurement, and the device was rinsed 3 times using DI water and air dried before platinum was sputtered on it for SEM observation. No Cp. oocysts were observed on the area outside of the graphene sheet.

In summary, large-size CVD grown graphene films configured as field-effect devices for sensing of Cp. oocysts with high sensitivity and specificity was demonstrated in this work. After the functionalization of the graphene device with the linker molecule and immobilization of specific antibody, the presence of Cp. oocysts can be detected by either (1) the change of the transfer curves, i.e., the dependence of drain current on the sweep of the gate voltage, or (2) real-time monitoring of the drain current change under a constant gate voltage. This study demonstrated the graphene field-

effect device as a promising candidate for the rapid detection of the Cp. oocysts with high sensitivity and specificity, and the biofunctionalized graphene device platform can be applied in the sensing of other bacterial, viral, protozoan waterborne pathogens and play important roles in water quality control.

This work was supported by Singapore University of Technology and Design–Zhe Jiang University joint pilot research project (SUTD-ZJU/PILOT/01/2011). X. C. Dong would like to acknowledge the financial support from Jiangsu Provincial Funds for Distinguished Young Scholars (SBK201310284), NNSF of China (21275076, 61328401), the Key Project of Chinese Ministry of Education (212058), and Research Fund for the Doctoral Program of Higher Education of China (20123223110008).

- <sup>1</sup>F. Schedin, A. K. Geim, S. V. Morozov, E. W. Hill, P. Blake, M. I. Katsnelson, and K. S. Novoselov, *Nature Mater* **6**, 652–655 (2007).
- <sup>2</sup>Y. W. Tan, Y. Zhang, K. Bolotin, Y. Zhao, S. Adam, E. H. Hwang, S. Das Sarma, H. L. Stormer, and P. Kim, *Phys. Rev. Lett.* **99**, 246803 (2007).
- <sup>3</sup>S. Chen, W. Cai, R. D. Piner, J. W. Suk, Y. Wu, Y. Ren, J. Kang, and R. S. Ruoff, *Nano Lett.* **11**, 3519–3525 (2011).
- <sup>4</sup>Y. Huang, X. Dong, Y. Shi, C. M. Li, L.-J. Li, and P. Chen, *Nanoscale* **2**, 1485–1488 (2010).
- <sup>5</sup>X. Dong, Y. Shi, W. Huang, P. Chen, and L.-J. Li, *Adv. Mater.* **22**, 1649–1653 (2010).
- <sup>6</sup>Y. Ohno, K. Maehashi, Y. Yamashiro, and K. Matsumoto, *Nano Lett.* **9**, 3318–3322 (2009).
- <sup>7</sup>S. He, B. Song, D. Li, C. Zhu, W. Qi, Y. Wen, L. Wang, S. Song, H. Fang, and C. Fan, *Adv. Funct. Mater.* **20**, 453–459 (2010).
- <sup>8</sup>C.-H. Lu, H.-H. Yang, C.-L. Zhu, X. Chen, and G.-N. Chen, *Angew. Chem. Int. Ed.* **48**, 4785–4787 (2009).
- <sup>9</sup>M. S. Abrahamsen, T. J. Templeton, S. Enomoto, J. E. Abrahante, G. Zhu, C. A. Lancto, M. Deng, C. Liu, G. Widmer, S. Tzipori, G. A. Buck, P. Xu, A. T. Bankier, P. H. Dear, B. A. Konfortov, H. F. Spriggs, L. Iyer, V. Anantharaman, L. Aravind, and V. Kapur, *Science* **304**, 441–445 (2004).
- <sup>10</sup>O. D. Simmons, M. D. Sobsey, C. D. Heaney, F. W. Schaefer, and D. S. Francy, *Appl. Environ. Microbiol.* **67**, 1123–1127 (2001).
- <sup>11</sup>C. K. Nielsen and L. A. Ward, *J. Vet. Diagn. Invest.* **11**, 567–569 (1999).
- <sup>12</sup>A. J. Alles, M. A. Waldron, L. S. Sierra, and A. R. Mattia, *J. Clin. Microbiol.* **33**, 1632–1634 (1995).
- <sup>13</sup>G. Vesey, P. Hutton, A. Champion, N. Ashbolt, K. L. Williams, A. Warton, and D. Veal, *Cytometry* **16**, 1–6 (1994).
- <sup>14</sup>R. A. Guy, P. Payment, U. J. Krull, and P. A. Horgen, *Appl. Environ. Microbiol.* **69**, 5178–5185 (2003).
- <sup>15</sup>C. Kaucner and T. Stinear, *Appl. Environ. Microbiol.* **64**, 1743–1749 (1998).
- <sup>16</sup>R. Fayer, U. Morgan, and S. J. Upton, *Int. J. Parasitol.* **30**, 1305–1322 (2000).
- <sup>17</sup>D. J. Cole, K. Snowden, N. D. Cohen, and R. Smith, *J. Clin. Microbiol.* **37**, 457–460 (1999).
- <sup>18</sup>See supplementary material at <http://dx.doi.org/10.1063/1.4864154> for graphene growing process, micro-channel fabrication procedure, Figures S1 and S2 and Table S1.
- <sup>19</sup>V. Georgakilas, M. Otyepka, A. B. Bourlinos, V. Chandra, N. Kim, K. C. Kemp, P. Hobza, R. Zboril, and K. S. Kim, *Chem. Rev.* **112**, 6156–6214 (2012).
- <sup>20</sup>K. Ostrikov, E. C. Neyts, and M. Meyyappan, *Adv. Phys.* **62**, 113–224 (2013).
- <sup>21</sup>Y. P. Shan, P. B. Tiwari, P. Krishnakumar, I. Vlasiouk, W. Z. Li, X. W. Wang, Y. Darici, S. M. Lindsay, H. D. Wang, S. Smirnov, and J. He, *Nanotechnology* **24**, 495102 (2013).
- <sup>22</sup>T. E. Saraswati, A. Ogino, and M. Nagatsu, *Carbon* **50**, 1253–1261 (2012).
- <sup>23</sup>J. Yang, F. Pang, R. Zhang, Y. Xu, P. He, and Y. Fang, *Electroanalysis* **20**, 2134–2140 (2008).
- <sup>24</sup>R. J. Chen, Y. Zhang, D. Wang, and H. Dai, *J. Am. Chem. Soc.* **123**, 3838–3839 (2001).
- <sup>25</sup>Y. Shi, X. Dong, P. Chen, J. Wang, and L.-J. Li, *Phys. Rev. B* **79**, 115402 (2009).
- <sup>26</sup>I. Heller, A. M. Janssens, J. Mannik, E. D. Minot, S. G. Lemay, and C. Dekker, *Nano Lett.* **8**, 591–595 (2008).
- <sup>27</sup>K. Besteman, J.-O. Lee, F. G. M. Wiertz, H. A. Heering, and C. Dekker, *Nano Lett.* **3**, 727–730 (2003).
- <sup>28</sup>X. P. A. Gao, G. Zheng, and C. M. Lieber, *Nano Lett.* **10**, 547–552 (2010).